ORIGINAL ARTICLE



Computational modeling predicts regulation of central pattern generator oscillations by size and density of the underlying heterogenous network

Iulian Ilieş¹ • Günther K. H. Zupanc¹

Received: 29 August 2021 / Revised: 12 September 2022 / Accepted: 18 September 2022 / Published online: 6 October 2022 © The Author(s), under exclusive licence to Springer Science+Business Media, LLC, part of Springer Nature 2022

Abstract

Central pattern generators are characterized by a heterogeneous cellular composition, with different cell types playing distinct roles in the production and transmission of rhythmic signals. However, little is known about the functional implications of individual variation in the relative distributions of cells and their connectivity patterns. Here, we addressed this question through a combination of morphological data analysis and computational modeling, using the pacemaker nucleus of the weakly electric fish Apteronotus leptorhynchus as case study. A neural network comprised of 60-110 interconnected pacemaker cells and 15–30 relay cells conveying its output to electromotoneurons in the spinal cord, this nucleus continuously generates neural signals at frequencies of up to 1 kHz with high temporal precision. We systematically explored the impact of network size and density on oscillation frequencies and their variation within and across cells. To accurately determine effect sizes, we minimized the likelihood of complex dynamics using a simplified setup precluding differential delays. To identify natural constraints, parameter ranges were extended beyond experimentally recorded numbers of cells and connections. Simulations revealed that pacemaker cells have higher frequencies and lower within-population variability than relay cells. Within-cell precision and between-cells frequency synchronization increased with the number of pacemaker cells and of connections of either type, and decreased with relay cell count in both populations. Network-level frequency-synchronized oscillations occurred in roughly half of simulations, with maximized likelihood and firing precision within biologically observed parameter ranges. These findings suggest the structure of the biological pacemaker nucleus is optimized for generating synchronized sustained oscillations.

Keywords Apteronotus leptorhynchus \cdot Central pattern generator \cdot Computational modeling \cdot Neural network \cdot Pacemaker nucleus \cdot Weakly electric fish

1 Introduction

Central pattern generators (CPGs) are neural networks that can produce rhythmic activity without cues provided by sensory feedback or input mediated by descending neurons (for reviews, see Bucher, 2009; Frigon, 2012; Grillner, 2006; Guertin, 2009; Katz, 2016; Marder & Bucher, 2001; Selverston, 2010). Their periodic output activity underlies,

Communicated by Action Editor: Catherine E Carr

 ☑ Günther K. H. Zupanc g.zupanc@northeastern.edu
 Iulian Ilieş i.ilies@northeastern.edu

¹ Laboratory of Neurobiology, Department of Biology, Northeastern University, Boston, MA 02115, USA in both invertebrates and vertebrates, numerous rhythmic behaviors, including respiration, locomotion (walking, flying, swimming), and gut movements. A characteristic feature of CPGs is their heterogenous cellular composition, with the involved cell types showing differences in morphological features, molecular signatures, electrophysiological properties, and synaptic input or output patterns (for review, see Hudson et al., 2010).

The relative contributions of the different cell types, including their synaptic connectivity patterns, have a major impact on the activity of the network, and thus on the behavioral function controlled by CPGs, as shown in the stomatogastric ganglion of decapod crustaceans (Harris-Warrick et al., 1992; Hudson et al., 2010) and in the pre-Bötzinger complex of mammals (Garcia et al., 2011). However, until now it has remained elusive (i) whether any inter-individual differences exist in absolute or relative numbers of different

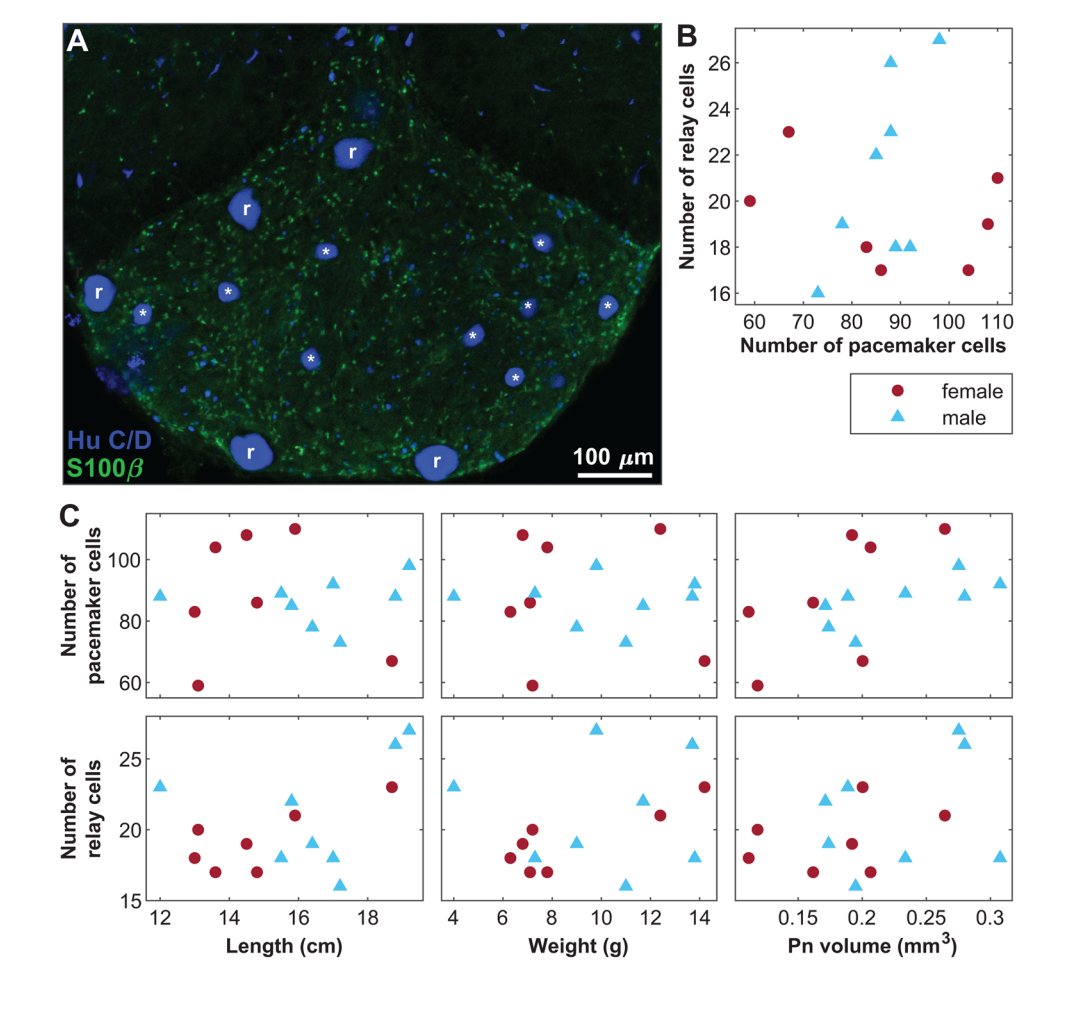


cell types and neuronal connections, and (ii) what the functional consequences of such morphological variability are in a given CPG.

In the present study, we addressed these issues by combining quantitative morphological analysis with computational modeling, using the pacemaker nucleus (Pn) of the weakly electric fish Apteronotus leptorhynchus as a wellestablished CPG. Like other apteronotids, this species features an electric organ formed by massively enlarged axonal terminals of electromotoneurons derived from spinal motoneurons (Bennett, 1971; de Oliveira-Castro, 1955; Waxman et al., 1972). Electric organ discharges (EODs) are produced by synchronous depolarization of the individual electrogenic cells. Discharges are generated continuously at frequencies of up to 1 kHz, reaching amplitudes of several hundred millivolts. As the duration of the electric pulse is comparable to the interpulse interval, the resulting discharge pattern resembles a train of quasi-sinusoidal electric signals. The frequency of the EOD of individual fish is highly constant (Bullock, 1969, 1970; Moortgat et al., 1998), surpassing in its stability any other known periodic signal generated by biological systems. The base EODs, together with complex transient frequency and amplitude modulations of the discharges during electric interactions (Dunlap et al., 1998; Engler & Zupanc, 2001; Zupanc & Maler, 1993; Zupanc et al., 2006), play important roles in active electrolocation, species and sex recognition, as well as intraspecific communication (for review, see Zupanc, 2018; Zupanc & Bullock, 2005).

EODs are driven in a one-to-one fashion by volleys of command spikes from the Pn (for review, see Dye & Meyer, 1986). Axons from relay cells, its output neurons, descend from the medulla oblongata to form electrotonic junctions with the electromotoneurons in the spinal cord. Together with an additional population of approximately 90 interconnected pacemaker cells, the roughly 20 relay cells form the network that generates the intrinsic oscillations of the Pn (Fig. 1A) (Sîrbulescu et al., 2014). Each pacemaker cell synapses, via gap junctions, with a limited number of pacemaker and relay cells (Dye & Heiligenberg, 1987; Elekes & Szabo, 1985; Moortgat et al., 2000a). An isolated Pn can generate the basic EOD activity, whereas input from descending neural pathways is required for the production of transient modulations (Dye, 1988). The frequency of the basic Pn oscillations, and thus of the EOD, is determined by several factors, including intrinsic properties of the

Fig. 1 Morphology of the A. leptorhynchus Pn. (A) Immunolabeling against the neuronal marker Hu C/D (blue) uncovers two distinct populations of large neurons, pacemaker cells (*) and relay cells (r), as well as numerous small interneurons with no documented role in the generation of Pn oscillations. These neuronal types are embedded in a dense astrocytic syncytium, revealed by immunostaining against the glial cell marker S100 β (green). The counts of pacemaker and relay cells do not correlate across fish, differ between males (blue triangles) and females (red circles) (B), or correlate with an individual's length, weight, or Pn volume (C). Tissue processing, digital imaging, and cell count quantification as described previously (Sîrbulescu et al., 2014)





pacemaker and relay cells (e.g., size, ion channel densities), and the potassium buffering capacity of the extensive astrocytic syncytium enveloping them (Fig. 1A) (Hartman et al., 2021; Zupanc et al., 2014).

The quantitative analysis performed as part of this study revealed substantial variability in the morphological structure of the Pn network among individual fish. Computer simulations using a simplified model of the Pn, designed to minimize the likelihood of complex dynamics, identified frequency-synchronized, spontaneous, and sustained oscillations with high temporal precision within the range of morphological variability. These dynamics were characterized by all cells firing at the same frequency, though not necessarily in phase, consistently across time and with no external inputs. However, we found increasing absence of such oscillations when testing network structure parameter values beyond those found in biological samples, with the notable exception of (likely biologically unfeasible) very large, densely connected networks. Thus, the present investigation suggests that the structure of the biological Pn is optimized for generating frequency-synchronized spontaneous sustained oscillations.

2 Methods

2.1 Modeling of pacemaker and relay cells

Pacemaker and relay cells were modeled in NEURON version 8.0 (Hines & Carnevale, 1997) via Python version 3.8 (Hines et al., 2009), building upon previous models of the neural network of the Pn (Hartman et al., 2021; Lucas et al., 2019; Moortgat et al., 2000b; Zupanc et al., 2019). In line with these earlier models, each cell consisted of two cylindrical sections with sizes derived from morphological data: (i) somatic, with diameter and length set to the average diameter of the cell soma (Dye & Heiligenberg, 1987); (ii) axonal, with dimensions equal to corresponding

measurements of the initial segment (Elekes & Szabo, 1985; Heiligenberg et al., 1996) (Table 1). Consistent with prior studies, dendritic compartments were excluded from the model as they only receive inputs from other brain regions responsible for frequency modulation (Elekes & Szabo, 1985; Moortgat et al., 2000b).

Each cell section was divided into 1-µm long segments expressing Hodgkin-Huxley ion channels (Hodgkin & Huxley, 1952), with maximum conductances, equilibrium potentials, and other electrical properties based on prior modeling studies (Hartman et al., 2021; Moortgat et al., 2000b) (Table 1). Since somatic and axonal segments differed in morphological and/or electrical properties, small phase lags were induced within as well as between cells (see Fig. 1d in Hartman et al., 2021). Parameters for ion channel gate functions were set to NEURON defaults (i.e., giant squid axon, per Hodgkin & Huxley, 1952), consistent with previous Pn models. Ion channel kinetics were scaled to 27 °C, the average ambient water temperature in the natural habitat of this species. K⁺- and Na⁺-related parameters for somatic compartments were set to values most likely to result in sustained spontaneous oscillations with frequencies within biologically observed ranges for A. leptorhynchus (per Fig. 2 in Hartman et al., 2021). All other parameters, including ion channel dynamics of axonal compartments, were set to the values employed in Moortgat et al. (2000b), which were generally chosen to match experimental measurements of cell properties (e.g., input resistances) or action potential characteristics (e.g., spike width).

2.2 Modeling of pacemaker nucleus network

The Pn network was modeled as a random directed graph using the NetworkX package (version 2.5) within Python. Consistent with morphological data (Dye & Heiligenberg, 1987; Elekes & Szabo, 1985) and prior modeling work (Hartman et al., 2021; Moortgat et al., 2000b; Zupanc et al., 2019), the axons of pacemaker cells synapsed with relay cells as well as other pacemaker cells, whereas relay cells

Table 1 Morphological and biophysical parameters of model pacemaker and relay cells. Values were derived from experimental data (Dye & Heiligenberg, 1987; Elekes & Szabo, 1985; Heiligenberg et al., 1996) (italic) or based on previous modeling studies (Hartman et al., 2021; Moortgat et al., 2000b). Underlined: values observed to produce spontaneous oscillations at biologically relevant frequencies in Hartman et al. (2021). See Sect. 2.1 for more details

Parameter	Parameter					
Group	Name	Unit	Soma	Axon	Soma	Axon
Morphological measurements	Length	μm	32	42	76	35
	Diameter	μm	32	5	76	6
Electrical properties	Axial resistivity	Ω·cm	100	100	100	500
	Membrane capacitance	μF/cm ²	1	1	1	1
Channel conductances	Sodium maximum	S/cm ²	<u>1.3</u>	0.5	<u>0.9</u>	0.5
	Potassium maximum	mS/cm ²	<u>160</u>	20	<u>160</u>	50
	Leak	mS/cm ²	0.1	1	0.3	1
Equilibrium potentials	Sodium	mV	<u>+61</u>	<u>+61</u>	<u>+61</u>	<u>+61</u>
	Potassium	mV	<u>-61</u>	<u>-61</u>	<u>-61</u>	<u>-61</u>
	Leak	mV	-70	-70	-70	-70



did not make synaptic contact with either pacemaker cells or other relay cells. Consequently, the Pn network was generated as a union of two subgraphs: (i) a random directed graph, connecting pacemaker cells with a defined probability; and (ii) a random bipartite directed graph, linking pacemaker cells to relay cells with another defined probability. Given the lack of empirical data on axonal lengths of pacemaker cells, these network connections did not include any information on spatial distribution. Accordingly, action potential transmission delays were the same for all pairs of connected cells, decreasing the likelihood of complex dynamics.

To explore the impact of network size and density on Pn oscillation patterns, the numbers of pacemaker and relay cells were varied from 3 to 200 in 11 geometric steps, respectively from 2 to 80 in 9 geometric steps, and the average counts of pacemaker-to-pacemaker and pacemaker-to-relay connections were varied from 1 to 13 in increments of 2 (Table 2). Each combination of parameters was evaluated 10 times, using a different randomly generated graph in each case. To minimize the interference from other sources of variation in firing frequency, such as differences in action potential travel times from pre-synaptic neurons projecting to any individual cell in the network, we fixed all other controllable factors, including soma and axon dimensions, and initial conditions of Hodgkin-Huxley equations governing each cell segment.

2.3 Modeling of network synaptic connections

Consistent with experimental data (Elekes & Szabo, 1985; Yamamoto et al., 1989), synaptic connections between Pn cells were implemented as rectifying gap junctions with instantaneous rectification using the model description language NMODL (Hines & Carnevale, 2000). Gap junctions were modeled in NEURON as half-gap objects (Gutierrez & Marder, 2013) affixed to the last axonal segment of the presynaptic cell and the first somatic segment of the post-synaptic cell (Hartman et al., 2021). Their conductivity was set to vary from 0.5 to 10 nS proportionally to the membrane potential difference between the two cells, consistent with experimentally determined properties (Gutierrez & Marder,

Table 2 Experimentally manipulated pacemaker network structural parameters. Values in *italic* denote size parameters evaluated only at subsets of the corresponding density parameters due to natural constraints (pacemaker-pacemaker connections < pacemaker cells, and pacemaker-relay

connections ≤ relay cells)

	Notation	Values
Pacemaker cells	пр	3, 4, 6, 10, 16, 24, 37, 56, 86, 131, 200
Relay cells	nr	2, 3, 5, 7, 12, 20, 31, 50, 80
Pacemaker-pacemaker connections per cell	npp	1, 3, 5, 7, 9, 11, 13
Pacemaker-relay connections per cell	npr	1, 3, 5, 7, 9, 11, 13
	Relay cells Pacemaker-pacemaker connections per cell Pacemaker-relay	Relay cells nr Pacemaker-pacemaker npp connections per cell Pacemaker-relay npr



2013). Since there are no data on coupling strength differences between pacemaker cells connecting with other pacemaker cells, as opposed to relay cells, conductances for these two junction types were assumed to be the same. Using identical parameters for all modeled gap junctions additionally ensured they do not introduce phase delays between signals arriving to post-synaptic cells from phase-synchronized presynaptic cells.

2.4 Numerical simulation of activity patterns

Pn networks were simulated under spontaneous conditions only (i.e., without injecting current). Initial potentials (applied to all segments in all cells), simulation durations, and action potential detection thresholds were determined following simulation of a minimal network consisting of a pacemaker cell connected to a relay cell for 100 ms, with membrane potentials initialized at -60 mV. The first 33 ms of the preliminary simulation were discarded to minimize contamination by initial transient patterns. The initial potential for whole-network simulations was set to -60.7 mV, the minimum membrane potential recorded during this preliminary simulation (used here as a proxy for the resting value). All other initial conditions (e.g., ion channel gate variables) were set to NEURON defaults (giant squid axon) for all cells, in all conducted simulations (including the preliminary one). This ensured all modeled cells started near their steady state (limit cycle) in each whole-network simulation, decreasing the duration of initial transients and the likelihood of complex, non-stationary network dynamics. The action potential threshold was set to -10.2 mV, the average midpoint between the minimum and maximum potentials recorded in the preliminary simulation. The full simulation duration was set to 143 ms, corresponding to 100 interspike intervals of the slowest firing cell. Numerical simulations were performed on a Dell OptiPlex 9020 desktop computer equipped with a 4-core Intel Core i7 CPU at 3.4 GHz and 16 GB RAM, and on a Dell Precision T7810 workstation equipped with dual 10-core Intel Xeon CPUs at 2.2 GHz and 128 GB RAM. To decrease computation times, numerical integration was performed with a variable time step, using NEURON's adaptive integration feature.

2.5 Determination of oscillation frequencies

Membrane potential traces (minimal networks and a small sample of whole-network simulations, randomly selected from across the parameter search space) and action potential time stamps (all simulations) were collected from the somatic section of each model cell adjacently to the axonal section (equivalent to the axon hillock in the biological cell). Action potentials were defined as membrane potential crossovers from below to above the -10.2 mV activation threshold. Their time stamps were used to compute instantaneous firing frequencies as inverses of interspike intervals. The frequency of each cell was defined as its median instantaneous frequency. It was considered stable if (i) the slope of frequency versus time past the first third of the simulation (to exclude any initial transient periods) did not differ significantly from 0 (p < 0.01), and (ii) the timespan from the last action potential to the simulation end did not exceed the median interspike interval by more than 2 interquartile ranges (IQRs). The network frequency was similarly defined as the median across all cells. It was labeled stable if (i) the frequency of each cell was stable, and (ii) all network cells were frequency-synchronized, operationalized here as the frequency difference between the slowest and fastest firing cells not exceeding 1 Hz. This threshold was selected to account for numerical precision in interspike interval and firing frequency measurements, estimated at ~1 Hz based on inspection of membrane potential traces generated in NEU-RON using adaptive integration as part of previous studies and preliminary testing.

2.6 Statistical analysis of simulation outputs

To quantify the effects of network size and density on spontaneous oscillation frequencies of Pn cells and synchronization thereof, the following four metrics were computed for the full network, pacemaker cell subnetwork, and relay cell population: (i) median frequency across all applicable cells; (ii) frequency IQR across all cells; (iii) median of within-cell instantaneous frequency IQR, a measure of firing precision; and (iv) proportion of cells exhibiting stable sustained oscillations. While more complex measures of stability and synchronicity that can distinguish between more complex types of dynamical states are available (e.g., Borges et al., 2017; Lodi et al., 2020; Stiefel & Ermentrout, 2016), the selection above are easy to compute at scale, and sufficiently sensitive to common non-stationary patterns. For example, bursting, waves, multi-stability, and spiral-like behaviors would result in high within-cell IQRs, while increasing and damped oscillations would lead to statistically significant deviations from within-cell frequency stability. Thus, they enable the identification of parameter combinations leading to highprecision, frequency-synchronized network oscillations (all cells have nearly identical frequencies, very low IQRs, and do not show significant trends in frequency over time) – the primary research question of this study.

These metrics, along with network frequency stability (defined above) as direct measure of frequency-synchronized sustained oscillations, were analyzed using generalized linear models with polynomial designs (including linear and quadratic terms for main effects, and all pairwise and higher order interactions between the linear terms) and distributionappropriate (normal or binomial) link functions. Unfeasible parameter combinations (e.g., fewer relay cells than average pacemaker-to-relay connections) were excluded from the analysis. Independent variables (counts of cells and connections of each type) were centered to an average of 0 before analysis to enable accurate evaluation of nonlinear terms. Significance levels of model coefficient estimates were computed via conversion to t-statistics and adjusted for multiple testing using the Benjamini-Hochberg method. Coefficient absolute values were used as a measure of effect size for ranking of model terms (main and interactions). Corresponding standard errors are reported as measures of estimate precision, and are proportional to the residual error of the fitted linear model in each case (pooled across all observations, i.e., all network parameter sets and simulation replicates).

3 Results

3.1 Patterns of variation in the biological pacemaker nucleus network

The numbers of pacemaker and relay cells and their possible correlations to other morphological characteristics of A. leptorhynchus individuals have been investigated in 3 experimental studies to date. Dye and Heiligenberg (1987) reported Pn networks consisting of 97 ± 25 (average \pm SD) pacemaker cells and 25 ± 7 relay cells (n = 11 individuals), identifying 2 non-trivial associations with other metrics: a correlation of 0.89 between pacemaker cell count and fish size (n=8), and one of 0.61 between relay cell diameters and EOD frequency (n = 12). More recently, Zupanc et al. (2014) computed pacemaker cell counts of 120 ± 2 (average \pm SE) for males and 135 \pm 15 for females, and relay cells counts of 26 ± 2 and 24 ± 2 , respectively (n = 6), with no sex differences in the number or profile area of either cell type (p > 0.5). In a separate investigation, Sîrbulescu et al. (2014) reported networks including 87 ± 4 (average \pm SE) pacemaker cells and 20 ± 1 relay cells (n = 15), with neither count correlating significantly with fish size (p > 0.1).

We reanalyzed the data from the Sîrbulescu et al. (2014) study, and found nearly twofold differences between the minimum and maximum counts of pacemaker (59 to 110) and relay cells (16 to 27). These findings are consistent with the



earlier report by Dye and Heiligenberg (1987), and indicate substantial inter-individual variability in the composition of this CPG. There was no correlation between the numbers of pacemaker and relay cells (p > 0.8; Fig. 1B), suggesting that Pn oscillations are not dependent on specific ratios between the two underlying cell populations. In addition, there was no correlation between either cell count and fish length, fish weight, or Pn volume (Fig. 1C; p > 0.05), nor were there any significant differences between male and female individuals (p > 0.3), suggesting that the empirically observed ranges of pacemaker and relay cell counts do not reflect morphological constraints.

3.2 Occurrence of frequency-synchronized spontaneous sustained oscillations

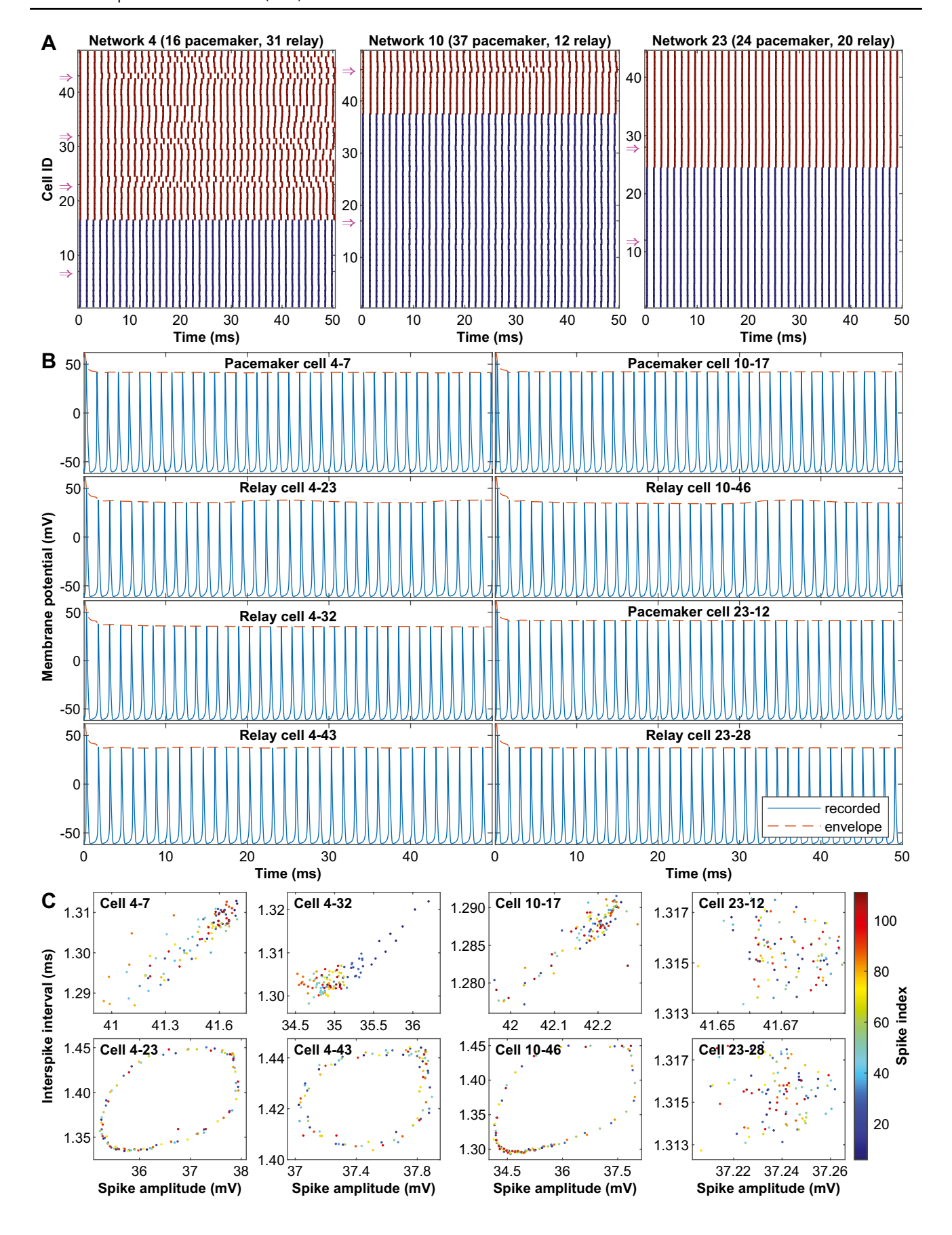
A systematic grid-based method, involving 2,640 parameter combinations, each evaluated at 10 randomly generated network graphs, was used for unbiased assessment of the effect of network size and density on Pn firing patterns in *A. leptorhynchus*. To identify any intrinsic constraints, parameters ranges were extended beyond biologically observed values (above), from minimal networks of 3 pacemaker and 2 relay cells or very sparse networks with one connection of each type per pacemaker cell, to twice the average numbers of pacemaker cells and connections and 4 times the average relay cell count.

Analysis of membrane potential recordings of pacemaker and relay cells from a selection of 25 parameter combinations revealed typically small initial transients and no complex network dynamics, in line with the simplified model setup. Since all simulated cells were able to produce stable sustained oscillations if left in isolation, networks with parameter configurations unable to result in frequency synchronization did not exhibit any time periods or subnetworks with no or substantially different activity levels. Instead, we observed individual cells firing at different, and in some instances non-constant, rates (Fig. 2). Correspondingly, frequency-locked cells appeared to be firing largely at the same time, up to a small delay between pacemaker and relay cells (Fig. 2A), as also observed in our prior work using the same model (Hartman et al., 2021). On average, modeled cells reached stability within 3 ms of simulation start, with only the first action potential and first interspike interval exceeding the value range (median ± 1.5 IQR) observed after the first third of the simulation, when firing patterns are stabilized (Fig. 2B). We did not find evidence of large-scale non-stationarity at the individual cell level, even in parameter combinations resulting in non-synchronized networks (20 out of the 25 examined). Typical deviations from frequency stability included low magnitude (up to about 10%) modulation of spike amplitude and firing Fig. 2 Example outputs of A. leptorhynchus Pn network model. A ▶ Spike raster plots of initial 50 ms of simulated neural activity of all pacemaker cells (dark blue) and all relay cells (dark red) within the modeled network for three different parameter combinations: left, small, relay-biased, densely-connected network, consisting of 16 pacemaker and 31 relay cells, with an average of 9 pacemaker-to-pacemaker and 9 pacemaker-to-relay junctions per pacemaker cell, and exhibiting largely desynchronized oscillations; middle, small, sparsely-connected network consisting of 37 pacemaker and 12 relay cells, with an average of 3 connections of each type per pacemaker cell, and showing predominantly frequency-synchronized oscillations; right, small, cell type balanced, densely-connected network comprised of 24 pacemaker and 20 relay cells, with an average of 13 connections of each type per pacemaker cell, and exhibiting frequency-synchronized oscillations. Each row corresponds to one cell (identifier shown on the vertical axis, ranging from 1 to 44-49). Magenta double arrows mark cells with membrane potential plots illustrated in more detail in **B-C**. For each cell in each network, vertical lines along the horizontal axis mark the times when its membrane potential crossed the action potential threshold (-10.2 mV) on an ascending trend. B Membrane potential (continuous blue line) and corresponding upper peak envelope (dashed red line) over time for representative pacemaker and relay cells from each of the networks in A. To facilitate interpretation, cells are labeled by their concatenated network and cell identifiers. Peak envelopes were obtained through spline interpolation of local maxima (= action potential peaks). C Scatter plots of interspike interval versus spike amplitude as a function of spike index for the representative cells shown in B. Spike amplitude was defined as the peak (maximum) membrane potential recorded during the action potential, with the corresponding interspike interval defined as the time from each such peak to the subsequent one. Individual measurements are color coded by spike index during the complete simulation (143 ms), ranging from 6 (dark blue) to 111 (dark red). The initial 5 spikes were conservatively removed from these plots to allow visualization of patterns and value ranges after initial transients. Relay cells 4-23, 4-43, and 10-46 show periodic changes in both interspike interval (firing frequency) and spike amplitude, with 10-46 showing a preference for values similar to those of pacemaker cells, while relay cell 4-32 slowly converges to the latter. Pacemaker cells 4-7 and 10-17, which are not as connected to other pacemaker cells as 23-12, show greater variation in interspike interval and spike amplitude, but no periodic trend. Note different scales on both horizontal and vertical axes across the different plots

frequency, and/or delayed convergence to pacemaker-like frequencies, in relay cells with too few inputs from pacemaker cells (Fig. 2C).

Quantitative analysis of network frequency stability measures uncovered widespread occurrence of frequency-synchronized sustained oscillations, with about 45% of the evaluated parameter combinations yielding networks comprised of cells firing within 1 Hz of each other consistently over time (Fig. 3). Frequency-synchronized oscillations were common within biologically observed parameter ranges (Fig. 3A) as well as in very large and densely connected networks (91% of all parameter combinations), but increasingly rarer in smaller networks (58%), and particularly so in large and weakly connected networks (21%) (Fig. 3B). Statistical analysis using a logistic model revealed very strong positive dependences on network connectivity with clear diminishing returns (manifested as large negative quadratic terms),







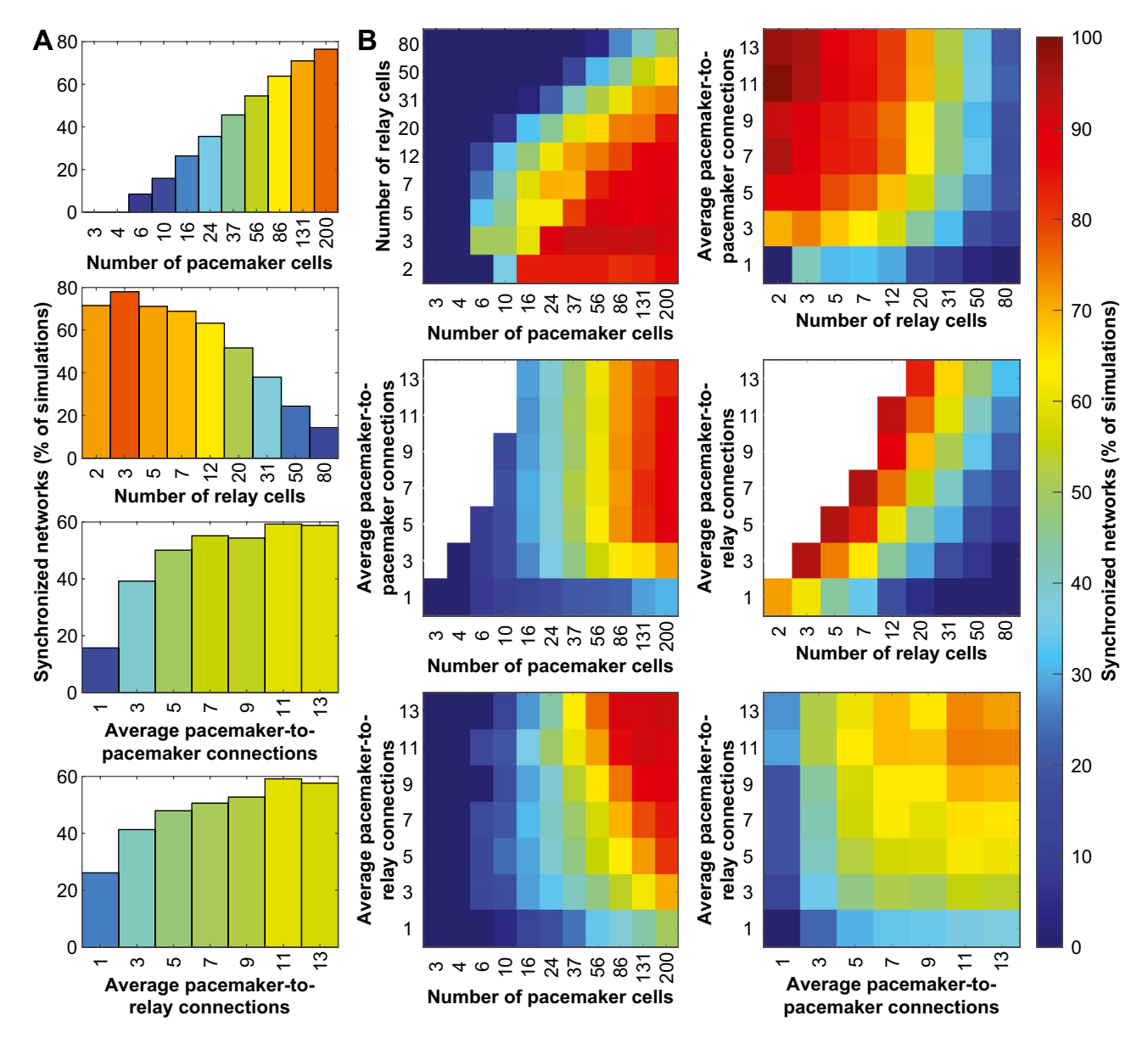


Fig. 3 Rate of frequency-synchronized sustained oscillations in the simulated *A. leptorhynchus* Pn as a function of network size (numbers of pacemaker and relay cells) and network density (average numbers of pacemaker-to-pacemaker and pacemaker-to-relay connections) parameters. Univariate (**A**) and bivariate (**B**) histograms show proportions (%) of parameter combinations yielding frequency-synchronized oscillations for each parameter value (bars in **A**) and for each pair of parameter values (pixels in **B**), pooled across replicates (10 randomly

generated networks per each parameter combination) and across all examined value combinations for the remaining parameters (44–540 in **A**, 1–99 in **B**). Bins are color coded by magnitude according to the scale shown to the right. Note different vertical axis scales in top two plots versus bottom two plots in **A**. White pixels in middle row plots in **B** mark unfeasible parameter combinations. Parameter values were sampled using geometric (cell counts) and linear (connection counts) grids (total of 2,640 combinations)

as well as a moderate negative dependence on the number of relay cells (Table 3), indicating that each cell requires a minimum number of inputs from other network cells in order to maintain frequency synchrony with the rest of the cells (Fig. 3B). This notion was additionally supported by significant positive interactions between each cell count and the corresponding number of incoming connections (Table 3).

3.3 Effects of network structure on population average firing frequencies

All examined network parameters significantly impacted the spontaneous oscillation frequencies of individual Pn cells, albeit in opposite directions depending on cell type (Table 4). The median frequency of pacemaker cells ranged



Table 3 Impact of network structure parameters and their interactions on the synchronization of sustained spontaneous oscillation frequencies within the *A. leptorhynchus* Pn network and the 2 neuronal subpopulations forming it. The network was considered frequency-synchronized if the firing frequency range across all cells did not exceed 1 Hz, and if no cell showed a statistically significant trend in frequency measurements over time (p < 0.01, linear regression). Analysis was performed

using a logistic regression model with linear and quadratic terms, as well as two-, three-, and four-way interactions. Reported values include regression coefficient estimates (β), corresponding standard errors (SE) and odds ratios (OR), and effect size ranks when statistically significant (p <0.05, adjusted for multiple comparisons using the Benjamini–Hochberg method). For parameter name abbreviations, see Table 2; —, not ranked (not significant)

Model factors		β	SE	OR	rank
Linear terms [/100]	пр	+9.19	0.17	1.096	4
	nr	-27.0	0.48	0.763	3
	npp	+51.0	1.89	1.665	2
	npr	+125	2.42	3.483	1
Quadratic terms [/1,000]	$np \times np$	-0.44	0.01	1.000	15
	$nr \times nr$	+1.53	0.10	1.002	11
	$npp \times npp$	-72.3	2.16	0.930	6
	$npr \times npr$	-83.8	3.18	0.920	5
Pairwise interactions [/1,000]	$np \times nr$	+1.05	0.06	1.001	13
	$np \times npp$	+1.38	0.29	1.001	12
	$np \times npr$	-2.45	0.33	0.998	10
	$nr \times npp$	+2.72	0.89	1.003	9
	$nr \times npr$	+17.8	1.06	1.018	7
	$n pp \times npr$	-11.1	4.38	0.989	8
Higher-order effects [/10,000]	$np \times nr \times npp$	-0.75	0.08	1.000	18
	$np \times nr \times npr$	-1.59	0.07	1.000	17
	$np \times npp \times npr$	+3.36	0.51	1.000	16
	$nr \times npp \times npr$	-7.47	1.24	0.999	14
	$np \times nr \times npp \times npr$	+0.03	0.02	1.000	_

from 755 to 826 Hz across tested parameter combinations, decreasing by 1.5 Hz for each additional pacemaker-torelay connection per pacemaker cell, and by 0.26 Hz for each pacemaker-to-pacemaker connection per cell or every 10 pacemaker cells, while increasing by 0.51 Hz for every 10 relay cells (Fig. 4). Correspondingly, the median relay cell frequency varied between 694 and 785 Hz, increasing by 0.41 Hz per pacemaker cell, and by 0.6 Hz per each additional pacemaker-to-pacemaker connection per cell (albeit with diminishing returns), decreasing by 0.8 Hz per relay cell, and exhibiting a quadradic-like dependence (sharp increase, then slow decrease) on the average number of pacemaker-to-relay connections (Fig. 4). Network-level patterns followed relay cell trends despite pacemaker cells being more numerous (average of 64 versus 32 cells), likely due to the stronger effect sizes. The analysis additionally uncovered many significant interactions in each cell population (Table 4), some with relatively high magnitudes (e.g., between the two average connection counts in both cell populations, and between the number of relay cells and the average number of pacemaker-to-relay connections at network level and in relay cells alone) - indicative of complex nonlinear dependencies between network structure parameters and Pn oscillation frequencies.

3.4 Effects of network structure on within-population frequency variability

Variability in firing frequency between pacemaker cells was generally very low, with a median population-level IQR of 0.13 Hz, 87% of the tested parameter combinations resulting in IQRs below 1 Hz, and 95% of observations below 2 Hz (Fig. 5). Statistical modeling uncovered many highly significant, but low magnitude dependencies, with the average number of pacemaker-to-pacemaker connections and the number of relay cells having the largest impacts, a roughly 0.07 Hz decrease per additional connection, respectively increase for every 5 relay cells (Table 5). By contrast, relay cells frequently showed greater variability in firing frequency, with similar global median (0.1 Hz) but 38% of the observations exceeding 1 Hz, and 10% exceeding 30 Hz (Fig. 5). Network structure significantly and nonlinearly impacted heterogeneity in relay cell frequencies, with the between-cells frequency IQR increasing by 0.28 Hz for each relay cell, and by 0.07 Hz per each additional pacemakerto-pacemaker connection, respectively decreasing by 1.1 Hz for each additional pacemaker-to-relay connection per pacemaker cell, and by 0.7 Hz for every 10 pacemaker cells within networks with at least 10 pacemaker cells (Table 5).



Table 4 Impact of network parameters on median firing frequencies in the *A. leptorhynchus* Pn network and the 2 neuronal populations forming it. Regression coefficients (β), corresponding standard errors (SE), and effect size ranks where statistically significant (p < 0.05, Benja-

mini-Hochberg adjustment) are given for linear and quadratic terms, as well as for two-, three-, and four-way interactions. Parameter name abbreviations as in Table 2; —, not ranked

Model factors		Pacema	ker cells		Relay ce	ells		Whole network		
Туре	Parameter / Effect	β	SE	rank	β	SE	rank	β	SE	rank
Linear terms [/100]	пр	-2.64	0.06	6	+40.9	0.25	4	+38.6	0.24	4
	nr	+5.08	0.13	4	-80.3	0.57	2	-59.7	0.55	2
	npp	-26.1	0.61	2	+60.0	2.59	3	+64.0	2.52	1
	npr	-150	0.66	1	+287	2.83	1	+50.5	2.75	3
Quadratic terms [/1,000]	$np \times np$	+0.35	0.01	14	-2.59	0.03	15	-2.61	0.03	13
Quantitate terms [r1,000]	$nr \times nr$	-0.05	0.04	_	+8.36	0.19	10	+4.49	0.18	11
	$npp \times npp$	+28.3	1.62	5	-66.1	6.94	6	-63.4	6.74	6
	$npr \times npr$	-1.85	1.70	_	-399	7.28	5	-92.6	7.07	5
Pairwise interactions [/1,000] $np \times nr$	$np \times nr$	-1.23	0.01	11	+3.63	0.06	13	+5.21	0.06	10
	$np \times npp$	+2.20	0.10	10	-7.81	0.41	11	-9.33	0.40	9
	$np \times npr$	+3.15	0.10	7	-19.3	0.41	9	-15.7	0.40	8
	$nr \times npp$	-2.37	0.23	9	-5.43	0.97	12	+2.98	0.94	12
	$nr \times npr$	+2.99	0.25	8	+42.5	1.07	7	+31.9	1.04	7
	$n pp \times npr$	-55.8	1.50	3	+38.0	6.41	8	+9.55	6.22	_
Higher-order effects [/10,000]	$np \times nr \times npp$	-0.03	0.04	_	+1.20	0.16	18	-0.36	0.15	_
	$np \times nr \times npr$	-1.65	0.04	15	+1.88	0.16	17	-4.50	0.15	15
	$np \times npp \times npr$	+7.90	0.24	13	-7.64	1.03	16	-1.92	1.00	_
	$nr \times npp \times npr$	-9.23	0.57	12	+29.9	2.46	14	+20.5	2.39	14
	$np \times nr \times npp \times npr$	+0.09	0.01	16	-0.47	0.04	19	-0.30	0.04	16

Higher order terms had low amplitude effect sizes, with the notable exception of a negative interaction between the two average connection counts (Table 5), indicating that the negative dependence of cell-to-cell frequency variability on pacemaker-to-pacemaker connectivity levels is accentuated for relay cell populations that receive few inputs from pacemaker cells, respectively reduced or even reversed for strongly connected relay populations. Network-level statistics again paralleled those observed for relay cells (Fig. 5), likely due to the much larger variation recorded in this population (nearly one order of magnitude difference).

3.5 Effects of network structure on within-cell frequency variability

Pacemaker and relay cells exhibited similar levels of within-cell frequency variability, reaching median IQRs of 1.1 and 1.3 Hz, and maximum IQRs of 80 and 52 Hz, respectively (Fig. 6). In both cell types, the within-cell IQR decreased with the number of pacemaker cells (by 0.71 Hz, respectively 0.89 Hz, for every 10 cells) and with the average count of pacemaker-to-pacemaker connections (by 0.34 Hz, respectively 0.15 Hz, for each additional connection), and increased

with the number of relay cells (by 0.1 Hz per cell for pacemaker cells, respectively 0.18 Hz for relay cells) (Table 6). By contrast, the average count of pacemaker-to-relay connections showed a differential effect, increasing within-cell IQRs in pacemaker cells by 0.1 Hz per connection, while greatly decreasing IQRs in relay cells, by an average of 0.77 Hz per additional connection. This difference was qualified by a similarly strong negative interaction between the two average connection counts in both cell types (Table 6), indicative of a diminished, respectively enhanced, impact of the average number of pacemaker-to-relay connections within Pn networks with dense pacemaker sub-networks, resulting in low within-cell IQRs for both cell populations in strongly connected networks. Further higher order terms with large magnitudes included quadratic terms for the two average connection counts in pacemaker cells (and, to a lesser degree, in relay cells), indicative of diminished effects for higher values (Fig. 6). Network-level results mirrored those obtained in pacemaker cells (Fig. 6, Table 6), likely due to the larger contribution as dominant cell type and broader range observed in this population. Taken together, these findings indicate that the pacemaker cell sub-network drives the Pn firing precision, with relay cells opposing this effect as they are added to the network.



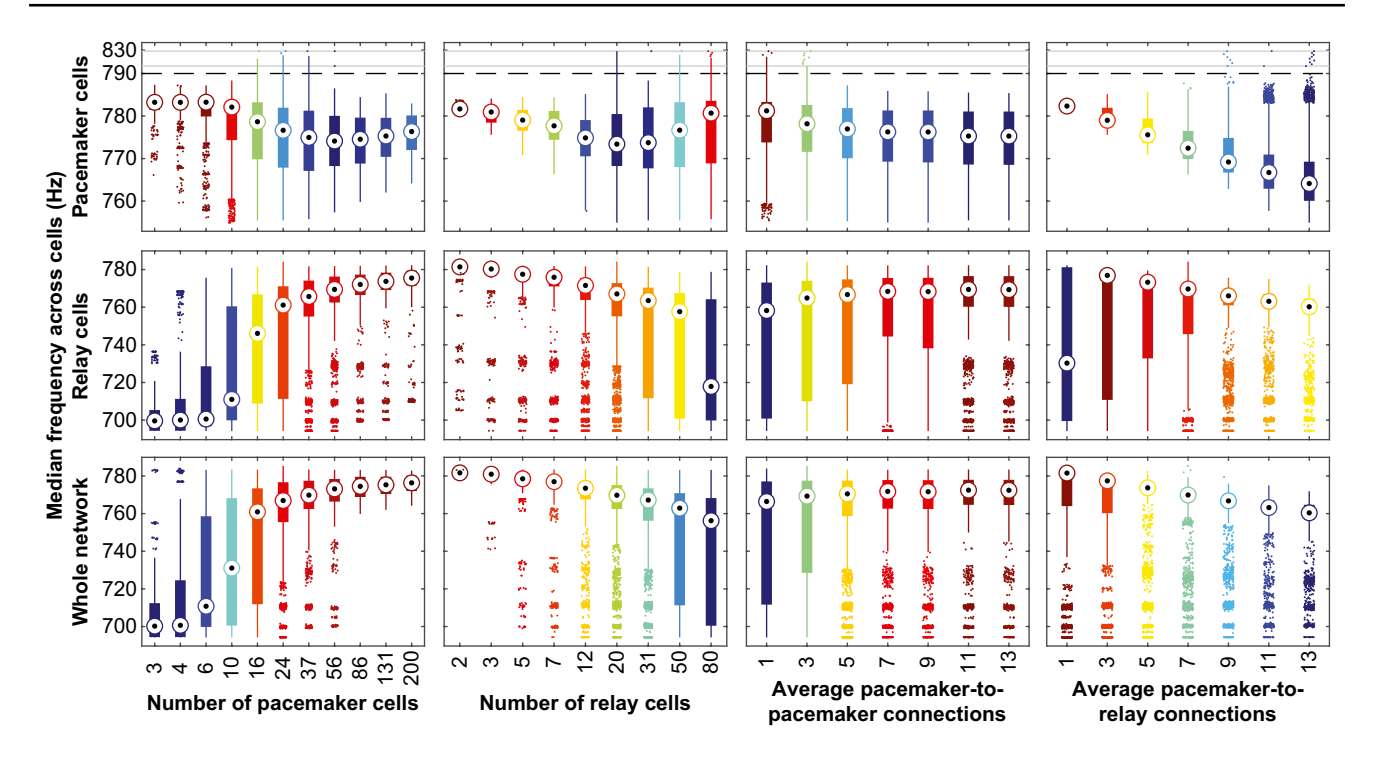


Fig. 4 Impact of network size and density on firing frequencies of cells in the *A. leptorhynchus* Pn network. Boxplots show distributions of within-population median frequencies for pacemaker cells (*top*), relay cells (*middle*), and the whole Pn network (*bottom*) for each tested value of each parameter (*columns*), pooled across replicates and value combinations of remaining parameters. *Solid boxes* mark the span between the lower and upper quartiles, with corresponding medians denoted by *black dots* inside *white circles*. *Whiskers* extend above and below each box to 1.5 interquartile ranges or the furthest data point in each direction, whichever is closest. Data points

beyond these values (outliers) are depicted by *colored dots*, with random noise added along the horizontal axis to minimize overlaps. To facilitate interpretation, extreme high outliers (values above the *dashed black line* in *top* plots) are compressed to a narrow section of the vertical axis (delimited by *continuous grey lines*), while boxes are color coded by median values, increasing from *dark blue* to *dark red* through *light green* (similar to the color map from Fig. 3), separately for each plot. Note different frequency scale for pacemaker cells (*top*) relative to relay cells and the whole network

3.6 Effects of network structure on within-cell frequency stability

Cell frequency stability, defined here as the slope of instantaneous frequency measurements over time being statistically indistinguishable from 0, was nearly universal, reaching averages of 97% in both pacemaker and relay cells across all parameter combinations (Fig. 7). Statistical analysis uncovered similar dependence patterns in these two populations, as well as for the Pn network as a whole (Table 7). The likelihood of frequency stability increased with the average number of pacemaker-to-pacemaker connections in a concave quadratic manner (sharp increase followed by gradual increase), while following a convex quadratic function with respect to the average count of pacemaker-torelay connections (first decreasing, then increasing). These patterns suggest the existence of a minimum connectivity threshold for the pacemaker cell sub-network, potentially moderated by the number of projections from pacemaker to relay cells. Most other terms showed negligible or nonsignificant effects (Table 7), with the exception of a negative interaction effect of increasing the average counts of both connection types simultaneously, most likely indicative of diminishing returns, and of small negative dependences on the counts of pacemaker and relay cells, possibly as a result of the increased chance to observe statistically significant trends in cell frequency when the number of tests performed (here, one per cell) becomes large.

4 Discussion

The present study investigated, to our knowledge for the first time, the impact of variations in the structure of the underlying neural network on the function of heterogeneous CPGs. Quantitative analysis indicated significant and uncorrelated variation in the numbers of pacemaker and relay cells in the Pn of *A. leptorhynchus*, reaching twofold ratios between the largest and smallest values observed, with no codependences to morphological measurements (e.g., fish length and weight). Prompted by these observations, we systematically explored the effects of pacemaker



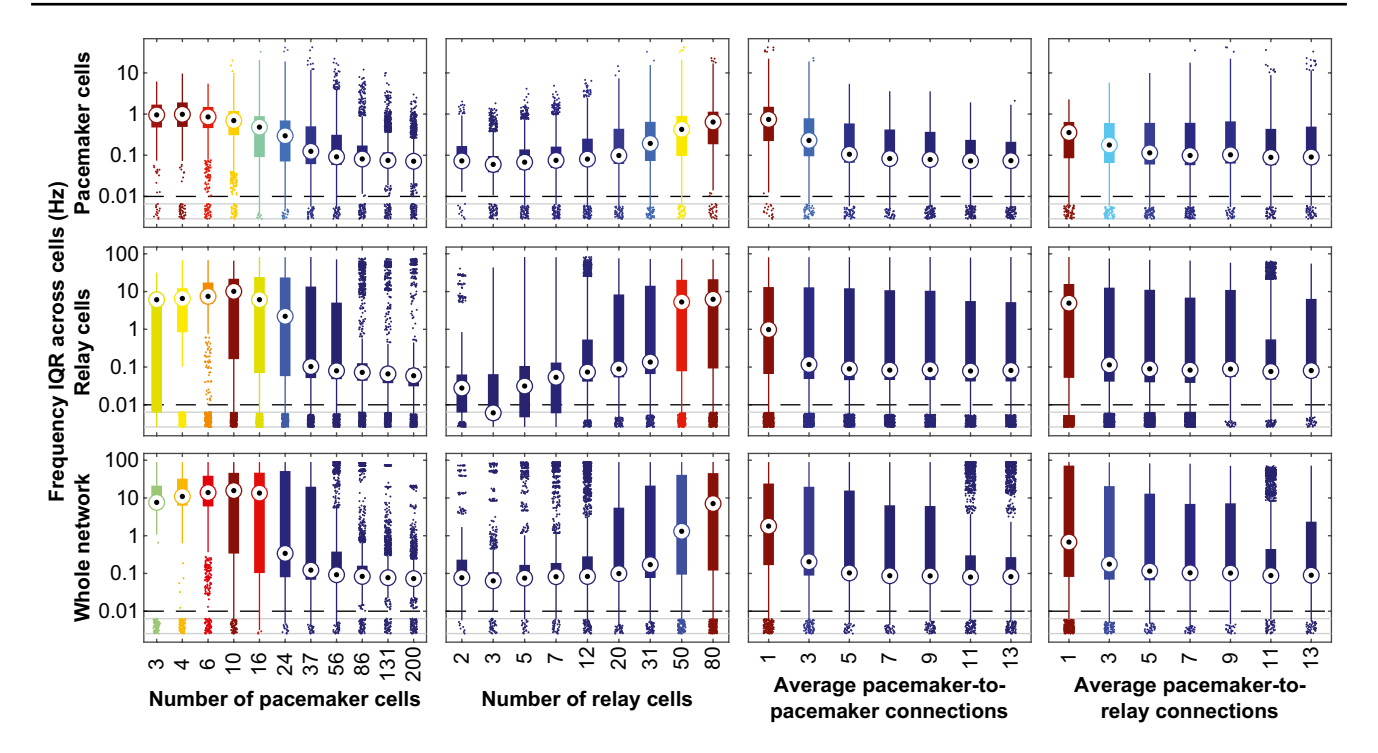


Fig. 5 Impact of network size and density on between-cells firing frequency variation in the *A. leptorhynchus* Pn network. Boxplots show distributions of population interquartile ranges (IQR) of frequencies for pacemaker cells (*top*), relay cells (*middle*), and the whole Pn network (*bottom*) as a function of the numbers of pacemaker (*left*) and relay (*center left*) cells, and average counts of pacemaker-to-pacemaker (*center right*) and pacemaker-to-relay (*right*) connections. Data were

combined across replicates and examined values of remaining parameters in each case. Box plot interpretation and color coding as in Fig. 4. To facilitate visualization, extreme low outliers (with values below dashed black line) are compressed to a narrow section of the vertical axis (marked by continuous grey lines). Note different frequency scale for pacemaker cells (top) compared to relay cells and the whole network. Note logarithmic vertical scale in all cases

and relay cell counts, and of average pacemaker-to-pacemaker and pacemaker-to-relay connection counts, on Pn oscillation frequencies and their variation across and within cells.

Computer simulations using parameter combinations well beyond biologically observed ranges uncovered numerous multilinear and polynomial dependencies of Pn oscillation patterns on the size and density of the underlying neural network and its constituent sub-networks. While a majority of cells across experiments were able to generate sustained oscillations at a consistent pace over time (Figs. 6–7), there was considerable variability in frequency, particularly between the two types (Figs. 4–5). Pacemaker cells fired at higher rates and with lower levels of between-cells variability relative to relay cells, with network-level oscillation patterns tilted toward either of the populations depending on their sizes and how tight they were connected to each other.

Notably, both within-cell firing precision (Fig. 6) and between-cells synchronization in frequency (Figs. 3, 5) increased with the counts of pacemaker cells and pacemaker-to-pacemaker and pacemaker-to-relay connections, while decreasing with the number of relay cells. Inspection of membrane potential recordings from individual cells uncovered

reduced frequency variability and increased action potential amplitude with additional incoming connections in both cell types (Fig. 2). Pacemaker cells with fewer connections from other pacemaker cells exhibited broader interspike interval distributions, while relay cells with insufficient inputs cycled between relay-like and pacemaker-like firing frequencies, tilting towards the latter as the number of incoming connections increases, then simply converging once they are numerous enough.

Overall, frequency IQRs for both cell types reached their minimum levels at the lower bound of experimentally determined pacemaker cell counts, respectively the upper bound of empirical numbers of relay cells (Figs. 4–5), indicating that the biological Pn is likely optimized for generating frequency-synchronized oscillations. Decreasing the number of pacemaker cells below about 50, e.g., to limit energy consumption, would dramatically reduce firing precision. Similarly, increasing the number of relay cells above 30, e.g., to enhance the signal provided to electromotoneurons, would also result in greatly decreased firing precision, unless proportionally incrementing the number of pacemaker cells or of pacemaker-to-relay connections, likely beyond biological feasibility ranges (Fig. 3B).



Table 5 Impact of network parameters on between-cells variation in firing frequency within the *A. leptorhynchus* Pn network and the 2 neuronal populations forming it. Between-cells variation was meas-

ured as the interquartile range of median instantaneous frequencies. Values given as in Table 4; parameter name abbreviations as in Table 2

Model factors		Pacema	ker cells	er cells Relay			Relay cells			Whole network		
Туре	Parameter / Effect	β	SE	rank	β	SE	rank	β	SE	rank		
Linear terms [/100]	пр	-0.49	0.02	5	-7.05	0.22	3	-20.6	0.34	3		
Linear ternis [/100]	nr	+1.41	0.03	2	+28.3	0.50	2	+51.0	0.76	2		
	npp	-7.59	0.16	1	+7.01	2.29	4	+4.86	3.48	_		
	npr	-0.85	0.17	4	-113	2.49	1	-267	3.79	1		
Quadratic terms [/1,000]	$np \times np$	+0.02	0.01	16	+0.34	0.03	17	+1.09	0.04	14		
Quadratic terms [/1,000]	$nr \times nr$	-0.13	0.01	13	-5.05	0.16	11	-7.42	0.25	9		
	$npp \times npp$	+12.0	0.42	3	-19.4	6.12	6	+9.69	9.30	_		
	$npr \times npr$	-2.26	0.44	7	+13.4	6.42	8	+186	9.76	4		
Pairwise interactions [/1,000]	1 1	-1.36	0.08	12								
Pairwise interactions [/1,000] $np \times np \times np \times np \times nr \times nr \times nr \times nr \times $	$np \times npp$	+0.34	0.02	10	-1.43	0.36	12	-2.11	0.55	11		
	$np \times npr$	-0.26	0.02	11	-5.60	0.36	10	+13.0	0.55	7		
	$nr \times npp$	-1.26	0.06	8	+11.2	0.86	9	+28.2	1.30	6		
	$nr \times npr$	+0.91	0.06	9	+13.8	0.95	7	-13.0	1.44	8		
	$n pp \times npr$	-4.22	0.38	6	-55.5	5.65	5	-78.6	8.59	5		
Higher-order effects [/10,000]	$np \times nr \times npp$	-0.01	0.01	_	-1.94	0.14	18	-4.80	0.21	15		
	$np \times nr \times npr$	-0.10	0.01	17	-4.77	0.14	15	-3.47	0.21	16		
	$np \times npp \times npr$	+1.15	0.06	14	+9.35	0.90	14	+12.3	1.37	13		
	$nr \times npp \times npr$	-1.89	0.15	12	+11.7	2.17	13	-30.4	3.30	10		
	$np \times nr \times npp \times npr$	+0.02	0.01	18	-0.17	0.03	19	+0.43	0.05	17		

4.1 Quantitative morphological analysis across different studies

Our quantitative morphological characterization of pacemaker and relay cell populations in the Pn of A. leptorhynchus is in good agreement with previous studies (Dye & Heiligenberg, 1987; Sîrbulescu et al., 2014; Zupanc et al., 2014). Besides confirming several earlier findings, it adds some notable details to the knowledge of Pn morphology, particularly in terms of inter-individual variability. Each of the four investigations has reported similar mean ratios of pacemaker to relay cells, as well as distinct, non-overlapping somatic size distributions for these two neuronal types. Using retrograde tracing from the spinal cord, Dye and Heiligenberg (1987) demonstrated that backfilled cells in the Pn (i.e., cells with the projecting pattern of relay cells) belong exclusively to the large-sized cell population, providing strong evidence that relay and pacemaker cells in the Pn can be distinguished unambiguously by difference in size.

On the other hand, a discrepancy exists between the Dye and Heiligenberg (1987) study and the analyses carried out by our laboratory previously (Sîrbulescu et al., 2014; Zupanc et al., 2014) and in the present study. Whereas we failed to detect any significant correlation between the numbers of the pacemaker or relay cells and fish size (defined by either total length or body weight), Dye and Heiligenberg (1987)

reported a significant correlation between fish size and number of pacemaker cells in the Pn, suggesting new pacemaker cells are added as the fish get older. It is likely that this discrepancy can be explained by differences in the composition of the samples taken. While body weight ranged from 1.3 to 15.7 g in the Sîrbulescu et al. (2014) and the present study, the sample collected by Dye and Heiligenberg (1987) was biased towards much larger fish, ranging from 6.8 to 60.4 g. It is, therefore, possible that age-related differences in the number of pacemaker cells become evident only when very large fish are included in the analysis, a size they reach near the end of their life expectancy.

4.2 Methodological considerations

The present analysis used nonparametric measures of central tendency (median) and dispersion (IQR), rather than the commonly employed average and SD, SE, or coefficient of variation (CV), to guard against outlier measurements due to irregular neuronal firing patterns. With over 2,600 parameter combinations screened, many that did not result in frequency-synchronized or stable oscillations, and with no a priori information on which combinations might yield such outcomes (given the stochasticity of randomly generated network structures), using nonparametric statistics provided a way to generate robust measurements that can



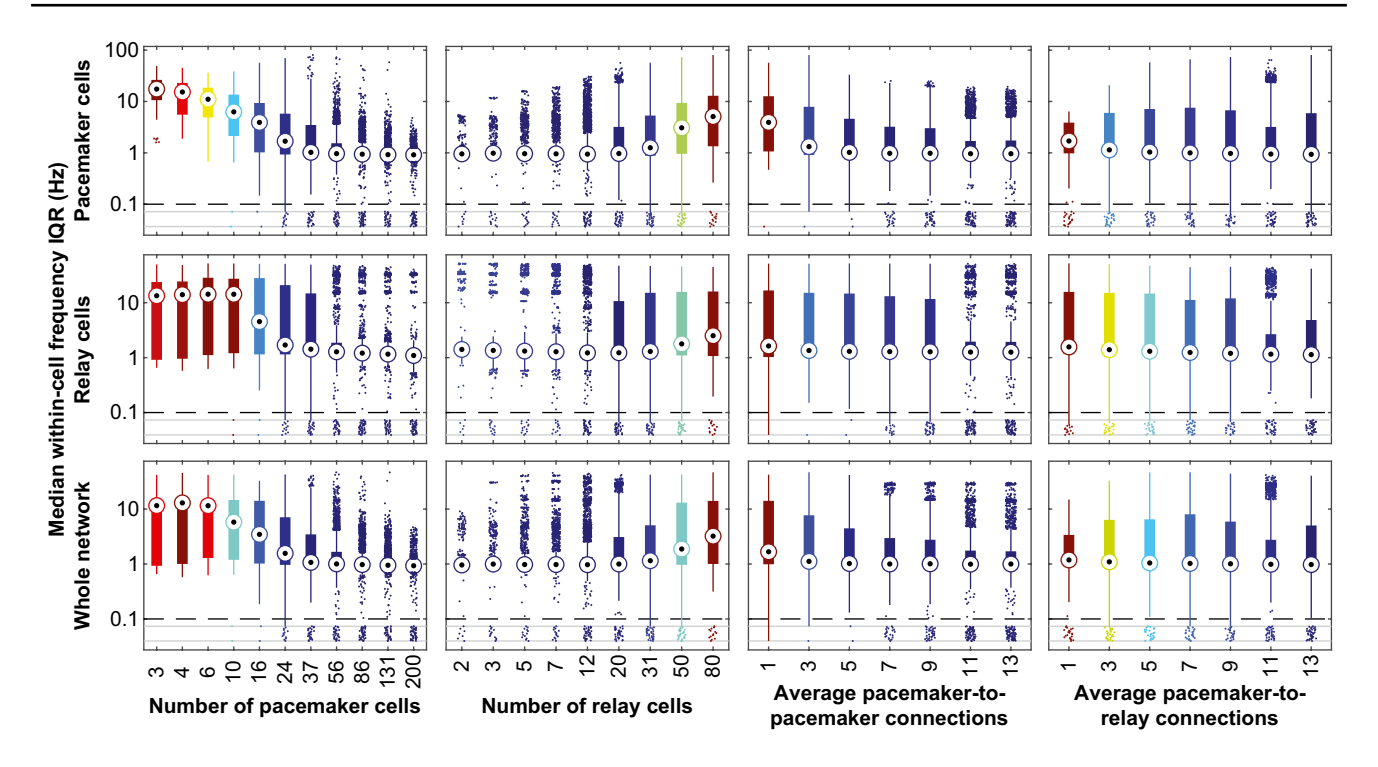


Fig. 6 Impact of network size and density on within-cell variation in firing frequencies in the *A. leptorhynchus* Pn network. Boxplots illustrate distributions of between-cells medians of within-cell interquartile ranges (IQR) of instantaneous frequencies for pacemaker cells (*top*), relay cells (*middle*), and the whole network (*bottom*) for each individual value of each parameter (*columns*). Data were pooled

across replicates and value combinations of remaining parameters in each case. Box plot interpretation, outlier scaling, and color coding as in Fig. 5. Note logarithmic vertical scale in all cases, and different frequency scale for pacemaker cells (*top*) relative to relay cells and the whole network

be safely aggregated across cells and experiments. Importantly, these statistics can be easily converted to their usual counterparts if the underlying data are well-behaved (e.g., mean = median, SD $\approx 3/4$ IQR, CV $\approx 4/3$ median/IQR for Gaussian distributions). Additionally, using nonparametric measures also alleviated the need to (manually or automatically) account for short-duration transient patterns at simulation start with no data loss – neither of the reported statistics are affected by initial outlier interspike intervals.

We relied on frequency synchronization as primary measure of cell population coherence, rather than the related but more restricted notion of phase synchronization, for several theoretical and computational reasons. First, based on our previous work (Hartman et al., 2021; Zupanc et al., 2019), we anticipated that firing frequencies of individual pacemaker and relay cells might vary substantially, particularly within weakly connected Pn networks. While frequency synchronized networks might exhibit a variety of temporal alignment patterns, e.g., a mix of time-synchronous and anti-synchronous cells, and arbitrary phase shifts for each cell, phase synchrony necessitates frequency synchrony. Second, observation of phase synchrony in the simplified model used here, with axons limited to their initial segments,

would not necessarily translate to the biological Pn, which features axons with variable lengths that might introduce differential delays. Conversely, phase synchrony of relay cell neural signals within the spinal cord, as needed to drive the EOD, or at the point where the relay cell axons exit the Pn, might not require phase synchrony between pacemaker and relay cell soma, given the variability in action potential travel times along axons with varying lengths and electric properties. Third, our previous results using the same modeling paradigm (Hartman et al., 2021) indicated no noticeable phase shifts, except in weakly connected relay cells. Fourth, accurately quantifying phase differences at high firing rates (700–800 Hz) would require very precise action potential timing data (i.e., very small integration time steps) or very large sample sizes (e.g., thousands of interspike intervals), which would be computationally prohibitive, particularly for larger networks. Fifth, inspection of membrane potential traces from a random set of simulations exhibiting desynchronized Pn networks did not reveal any complex dynamics (e.g., bursting) whose identification might require more advanced frequency or phase measures.

Finally, due to the focus on network topology, the present model used simplified neurons with identical geometries and



Table 6 Impact of network parameters on within-cell variation in firing frequency within the *A. leptorhynchus* Pn network and the 2 neuronal populations forming it. Within-cell variation was measured as the

median of within-cell interquartile ranges of instantaneous frequencies. Values given as in Table 4; parameter name abbreviations as in Table 2

Model factors		Pacemaker cells			Relay cells			Whole network		
Туре	Parameter / Effect	β	SE	rank	β	SE	rank	β	SE	rank
Linear terms [/100]	пр	-7.05	0.06	4	-8.90	0.16	4	-7.10	0.08	4
	nr	+10.2	0.14	3	+17.7	0.37	2	+9.62	0.19	3
	npp	-33.9	0.63	1	-15.2	1.67	3	-25.6	0.87	1
	npr	+10.4	0.69	2	-77.4	1.82	1	+14.6	0.95	2
Quadratic terms [/1,000]	$np \times np$	+0.51	0.01	16	+0.56	0.02	14	+0.49	0.01	14
Q	$nr \times nr$	-0.64	0.05	14	-3.12	0.12	10	-1.09	0.06	12
	$npp \times npp$	+39.7	1.68	6	+13.3	4.48	6	+24.7	2.33	7
	$npr \times npr$	-35.4	1.77	7	+9.53	4.70	9	-60.3	2.44	5
Pairwise interactions [/1,000]	$np \times nr$	-0.85	0.02	12	+0.28	0.04	16	-0.46	0.02	15
	$np \times npp$	+3.41	0.10	10	+1.14	0.26	12	+2.31	0.14	11
	$np \times npr$	-2.51	0.10	11	-2.58	0.27	11	-3.39	0.14	10
	$nr \times npp$	-3.76	0.24	9	+11.2	0.63	8	+5.38	0.33	9
	$nr \times npr$	+8.03	0.26	8	+11.8	0.69	7	+9.09	0.36	8
	$n pp \times npr$	-52.6	1.56	5	-67.1	4.13	5	-53.0	2.15	6
Higher-order effects [/10,000]	$np \times nr \times npp$	+0.06	0.04	_	-2.18	0.10	17	-1.38	0.05	17
	$np \times nr \times npr$	-0.94	0.04	17	-3.61	0.10	15	-0.94	0.05	18
	$np \times npp \times npr$	+8.36	0.25	13	+10.9	0.66	13	+8.79	0.34	13
	$nr \times npp \times npr$	-6.09	0.60	15	+3.33	1.59	_	+3.25	0.82	16
	$np \times nr \times npp \times npr$	+0.06	0.01	18	-0.06	0.03	18	-0.06	0.01	19

initial conditions, axons restricted to their initial segments, and gap junctions with identical localization and conductivity. These design choices ensured the modeled cells and junctions do not induce differential phase lags between synchronous incoming signals, decreasing the likelihood of complex network dynamics such as waves, bursting, and prolonged transients (see fifth point above). While changes in electrical properties between somatic and axonal compartments can introduce small conduction delays between pre- and post-synaptic cells (Moortgat et al., 2000b) (see also Fig. 1d in Hartman et al., 2021), the homogeneous cell models (within each type) and simplified spatial layout used here resulted in short, uniform travel times of action potentials from one cell to the next. In combination with the identical initial conditions (no differential starts), this enabled the quantification of network size and density effects on Pn frequency synchronization independently from the impact of heterogeneities in the spatial layout and electrical properties of involved cells. Further research will be needed to determine whether the quantified effect sizes are diminished or augmented by interactions with such confounders in models with more realistic geometries and heterogeneity, as well as whether they translate from frequency synchrony to the more specific, but biologically relevant concept of phase synchrony (all cells fire at the same time) in such expanded models.

4.3 Impact of network structure on firing precision

Extensive theoretical work using multiple in silico systems has provided some insight into how heterogeneity of neural oscillators affects network dynamics (Brunel, 2000; Grabow et al., 2010, 2011; Tönjes et al., 2010; White et al., 1998). Most importantly, one of the cardinal features of heterogeneity network size — has been demonstrated to influence the precision of individual oscillators in CPGs and their synchronization. Congruently, early in vitro research using cultured ventricular cells from chicken (Clay & DeHaan, 1979) had found that cluster size has no impact on the average inter-beat interval, whereas beat-to-beat variation in this metric, as quantified by the CV, scaled inversely proportional to the square root of the number of cells in the cluster. Recent modeling studies have uncovered similar inverse square root dependencies of interspike interval variability, including for FitzHugh-Nagumo oscillators (Kori et al., 2012), circadian clock cells in the suprachiasmatic nucleus of mammals (Vasalou et al., 2009), and relay cells in the A. leptorhynchus Pn (Moortgat et al., 2000b).

Irregularities in CPG inter-beat intervals have been hypothesized to arise from membrane potential noise, e.g., stochastic opening and closing of ion channels (Clay & DeHaan, 1979). In cell culture clusters, membrane fluctuations can be shown to be roughly inversely proportional to cluster diameter, and thus to the square root of the cell



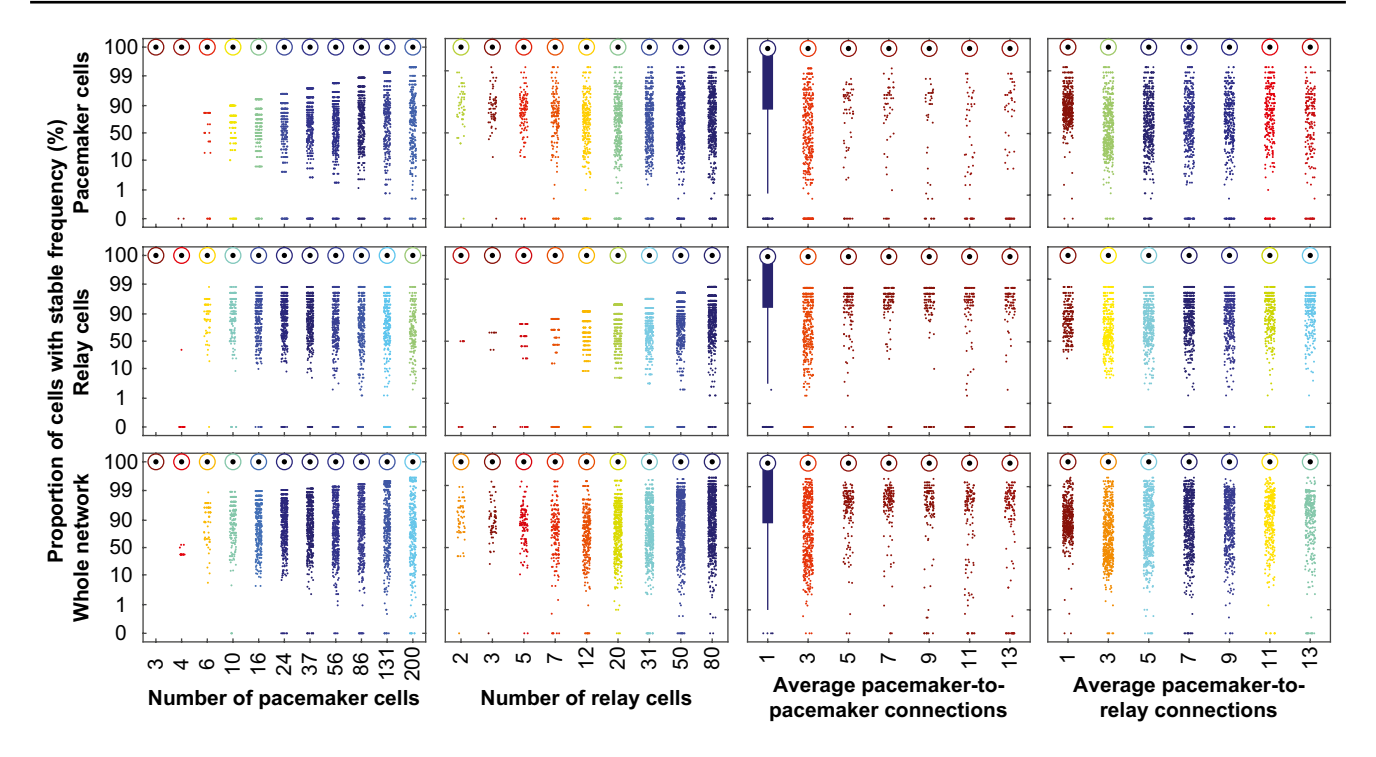


Fig. 7 Impact of network size and density on firing frequency stability in the *A. leptorhynchus* Pn network. Boxplots show the distributions of proportions of pacemaker cells (*top*), relay cells (*middle*), and pacemaker and relay cells combined (*bottom*), that did not show significant trends in instantaneous frequency over time, as a function of the numbers of pacemaker and relay cells (*left*) and the average num-

bers of pacemaker-to-pacemaker and pacemaker-to-relay connections (right). In each case, measurements were pooled across replicates and examined values of the remaining parameters. Box plot interpretation as in Fig. 4. Boxes are color coded by the fraction of observations equal to 1, increasing from dark blue to dark red through light green, separately for each plot. Note logit vertical scale in all cases

count, suggesting a possible dependence. Recent theoretical modeling (Kori et al., 2012) has identified the inverses of network size and of average connection strength as the variance components of membrane potential noise, supporting earlier postulates while also suggesting that increasing the number of cells cannot improve firing precision indefinitely. Subsequent numerical experiments found that CVs of interspike intervals scale with the inverse square root of network size only up to a system-specific maximum number of cells, which in turn increases with average coupling strength (Kori et al., 2012). These findings were consistent across topologies ranging from nearest-neighbors lattice to fully connected, with addition of long-range connections providing greater precision increases compared to local ones.

Connectivity patterns also play an important role in the emergence of network synchrony. Using CPG models consisting of sparsely connected integrate-and-fire neurons, two research groups (Golomb & Hansel, 2000; Tattini et al., 2012) have demonstrated that occurrence of (partially or fully) synchronized oscillations requires a minimum average connectivity. The critical number of connections grows logarithmically with network size, eventually converging to a constant value (Tattini et al., 2012), indicating that the minimal connectivity threshold is largely independent of

network density. The asynchronous state becomes unstable above this critical value (Golomb & Hansel, 2000), suggesting that coherent activity can spontaneously occur even in weakly coupled CPGs if each network cell receives enough inputs from other network cells. Accordingly, a small world topology (with small numbers of local connections and a few distant ones) may provide an optimal tradeoff between energy expenditure on signal transmission and control of firing patterns – including in more realistic heterogenous oscillator models (Vasalou et al., 2009).

The present study supports the natural condition that each CPG cell receives sufficiently many synapses from other network cells to allow synchronous activity, with additional incoming connections subject to diminishing returns. A secondary population of oscillators (here, the relay cells) might therefore be essential to transmit CPG output signals to the spinal cord, depending on local morphological conditions (e.g., available volume, axonal geometry constraints). While the core network (here, pacemaker cells) can generate highly precise oscillations if above some minimum size and density, the output cell population, with their weaker connectivity patterns and different morphologies (considerably larger somata, different ion channel densities) may act as a destabilizer and/or modulator. This notion is consistent



Table 7 Impact of network parameters on firing frequency stability within the *A. leptorhynchus* Pn network and the 2 neuronal populations forming it. Cell-level frequency stability was defined as absence

of statistically significant trends in instantaneous frequency measurements over time. Values given as in Table 4; parameter name abbreviations as in Table 2

Model factors		Pacema	ker cells		Relay ce	ells		Whole network		
Туре	Parameter / Effect	β	SE	rank	β	SE	rank	β	SE	rank
Linear terms [/100]	пр	-1.95	0.17	6	-1.57	0.16	6	-1.81	0.16	6
	nr	-1.87	0.52	7	-1.07	0.47	_	-1.57	0.50	7
	прр	+40.4	2.30	1	+31.8	2.00	1	+37.0	2.17	1
	npr	-22.5	2.78	2	-17.9	2.57	2	-20.9	2.69	2
Quadratic terms [/1,000]	$np \times np$	+0.19	0.01	13	+0.15	0.01	12	+0.17	0.01	13
Quadratic terms [/1,000]	$nr \times nr$	+0.82	0.08	11	+0.80	0.09	10	+0.81	0.08	11
	$npp \times npp$	-47.7	3.95	5	-45.3	3.90	3	-46.9	3.93	4
	$npr \times npr$	+49.6	3.83	3	+45.0	4.19	4	+48.6	4.02	3
Pairwise interactions [/1,000]	$np \times nr$	-0.34	0.06	12	-0.37	0.06	11	-0.34	0.06 12	12
Pairwise interactions [/1,000] $np \times nr$ $np \times npp$	$np \times npp$	-1.76	0.30	10	-1.11	0.28	9	-1.39	0.29	10
	$np \times npr$	+3.66	0.39	9	+3.10	0.38	8	+3.42	0.38	9
	$nr \times npp$	+1.33	1.01	_	+1.60	0.93	_	+1.01	0.97	_
	$nr \times npr$	-5.05	1.17	8	-6.38	1.11	7	-5.51	1.14	8
	$n pp \times npr$	-48.3	5.47	4	-35.8	5.04	5	-45.3	5.31	5
Higher-order effects [/10,000]	$np \times nr \times npp$	+0.34	0.12	14	+0.22	0.11	_	+0.31	0.12	14
	$np \times nr \times npr$	-0.31	0.13	_	-0.16	0.12	_	-0.25	0.13	_
	$np \times npp \times npr$	+0.15	0.69	_	+0.05	0.68	_	+0.14	0.69	_
	$nr \times npp \times npr$	+4.56	2.19	_	+0.92	1.95	_	+3.65	2.08	_
	$np \times nr \times npp \times npr$	-0.06	0.03	_	-0.03	0.02	_	-0.05	0.03	15

with the observation that chirping, a major type of transient EOD modulation, is mediated by excitatory input from the diencephalic prepacemaker nucleus to the relay cells (Heiligenberg et al., 1996). Taken together, the present findings indicate that the structural organization of the Pn network may lead to CPG performance trade-offs and functionally optimal ranges for the sizes of the two involved cell populations.

Acknowledgements The code file implementing the NEURON model is available in a public GitHub repository at the following link: https://github.com/LaboratoryOfNeurobiology/modeling-heterogeneous-cpg. We would like to thank Dr. Ruxandra F. Sîrbulescu for providing the confocal image of the *A. leptorhynchus* Pn shown in Figure 1A, and for helpful discussions. This research was supported by Grant 1946910 from the National Science Foundation (GKHZ).

Declarations

Conflict of interest The authors declare that they have no conflict of interest.

References

Bennett, M. V. L. (1971). Electric organs. In W. S. Hoar & D. J. Randall (Eds.), *Fish physiology, Vol. 5: Sensory systems and electric organs* (pp. 347–491). Academic Press.

Borges, F. S., Protachevicz, P. R., Lameu, E. L., Bonetti, R. C., Iarosz, K. C., Caldas, I. L., Baptista, M. S., & Batista, A. M. (2017). Synchronised firing patterns in a random network of adaptive exponential integrate-and-fire neuron model. *Neural Networks*, 90, 1–7.

Brunel, N. (2000). Dynamics of sparsely connected networks of excitatory and inhibitory spiking neurons. *Journal of Computational Neuroscience*, 8, 183–208.

Bucher, D. (2009). Central pattern generators. In L. R. Squire (Ed.), Encyclopedia of neuroscience (pp. 691–700). Academic Press.

Bullock, T. H. (1969). Species differences in effect of electroreceptor input on electric organ pacemakers and other aspects of behavior in electric fish. *Brain, Behavior and Evolution*, 2, 85–118.

Bullock, T. H. (1970). The reliability of neurons. *Journal of General Physiology*, 55, 565–584.

Clay, J. R., & DeHaan, R. L. (1979). Fluctuations in interbeat interval in rhythmic heart-cell clusters: Role of membrane voltage noise. *Biophysical Journal*, 28, 377–389.

de Oliveira-Castro, G. (1955). Differentiated nervous fibers that constitute the electric organ of *Sternarchus albifrons* Linn. *Anais Da Academia Brasileira De Ciências*, 27, 557–564.

Dunlap, K. D., Thomas, P., & Zakon, H. H. (1998). Diversity of sexual dimorphism in electrocommunication signals and its androgen regulation in a genus of electric fish, *Apteronotus*. *Journal of Comparative Physiology A*, 183, 77–86.

Dye, J. (1988). An in vitro physiological preparation of a vertebrate communicatory behavior: Chirping in the weakly electric fish, Apteronotus. Journal of Comparative Physiology A, 163, 445–458.

Dye, J., & Heiligenberg, W. (1987). Intracellular recording in the medullary pacemaker nucleus of the weakly electric fish, *Apteronotus*, during modulatory behaviors. *Journal of Comparative Physiology* A, 161, 187–200.



- Dye, J. C., & Meyer, J. H. (1986). Central control of the electric organ discharge in weakly electric fish. In T. H. Bullock & W. Heiligenberg (Eds.), *Electroreception* (pp. 71–102). John Wiley.
- Elekes, K., & Szabo, T. (1985). Synaptology of the medullary command (pacemaker) nucleus of the weakly electric fish (*Apteronotus leptorhynchus*) with particular reference to comparative aspects. *Experimental Brain Research*, 60, 509–520.
- Engler, G., & Zupanc, G. K. H. (2001). Differential production of chirping behavior evoked by electrical stimulation of the weakly electric fish, *Apteronotus leptorhynchus*. *Journal of Comparative Physiology A*, 187, 747–756.
- Frigon, A. (2012). Central pattern generators of the mammalian spinal cord. *The Neuroscientist*, 18, 56–69.
- Garcia, A. J., 3rd., Zanella, S., Koch, H., Doi, A., & Ramirez, J.-M. (2011). Networks within networks: The neuronal control of breathing. *Progress in Brain Research*, 188, 31–50.
- Golomb, D., & Hansel, D. (2000). The number of synaptic inputs and the synchrony of large, sparse neuronal networks. *Neural Com*putation, 12, 1095–1139.
- Grabow, C., Grosskinsky, S., & Timme, M. (2011). Speed of complex network synchronization. *European Physical Journal B*, 84, 613–626.
- Grabow, C., Hill, S. M., Grosskinsky, S., & Timme, M. (2010). Do small worlds synchronize fastest? *EPL*, *90*, 48002.
- Grillner, S. (2006). Biological pattern generation: The cellular and computational logic of networks in motion. *Neuron*, 52, 751–766.
- Guertin, P. A. (2009). The mammalian central pattern generator for locomotion. *Brain Research Reviews*, 62, 45–56.
- Gutierrez, G. J., & Marder, E. (2013). Rectifying electrical synapses can affect the influence of synaptic modulation on output pattern robustness. *Journal of Neuroscience*, 33, 13238–13248.
- Harris-Warrick, R., Marder, E., Selverston, A. I., & Moulins, M. (1992). *Dynamics biological networks*. MIT Press.
- Hartman, D., Lehotzky, D., Ilieş, I., Levi, M., & Zupanc, G. K. H. (2021). Modeling of sustained spontaneous network oscillations of a sexually dimorphic brainstem nucleus: The role of potassium equilibrium potential. *Journal of Computational Neuroscience*, 49, 419–439.
- Heiligenberg, W., Metzner, W., Wong, C. J. H., & Keller, C. H. (1996). Motor control of the jamming avoidance response of *Apteronotus leptorhynchus*: Evolutionary changes of a behavior and its neuronal substrates. *Journal of Comparative Physiology A*, 179, 653–674.
- Hines, M. L., & Carnevale, N. T. (1997). The NEURON simulation environment. *Neural Computation*, *9*, 1179–1209.
- Hines, M. L., & Carnevale, N. T. (2000). Expanding NEURON's repertoire of mechanisms with NMODL. Neural Computation, 12, 995–1007.
- Hines, M. L., Davison, A. P., & Muller, E. (2009). NEURON and Python. *Frontiers in Neuroinformatics*, 3, 1.
- Hodgkin, A. L., & Huxley, A. F. (1952). A quantitative description of membrane current and its application to conduction and excitation in nerve. *Journal of Physiology*, 117, 500–544.
- Hudson, A. E., Archila, S., & Prinz, A. A. (2010). Identifiable cells in the crustacean stomatogastric ganglion. *Physiology*, 25, 311–318.
- Katz, P. S. (2016). Evolution of central pattern generators and rhythmic behaviours. *Philosophical Transactions of the Royal Society* B, 371, 20150057.
- Kori, H., Kawamura, Y., & Masuda, N. (2012). Structure of cell networks critically determines oscillation regularity. *Journal* of Theoretical Biology, 297, 61–72.
- Lodi, M., Della Rossa, F., Sorrentino, F., & Storace, M. (2020). Analyzing synchronized clusters in neuron networks. *Scientific Reports*, 10, 16336.
- Lucas, K. M., Warrington, J., Lewis, T. J., & Lewis, J. E. (2019).Neuronal dynamics underlying communication signals in a

- weakly electric fish: Implications for connectivity in a pace-maker network. *Neuroscience*, 401, 21–34.
- Marder, E., & Bucher, D. (2001). Central pattern generators and the control of rhythmic movements. *Current Biology*, 11, R986–R996.
- Moortgat, K. T., Bullock, T. H., & Sejnowski, T. J. (2000a). Precision of the pacemaker nucleus in a weakly electric fish: Network versus cellular influences. *Journal of Neurophysiology*, 83, 971–983.
- Moortgat, K. T., Bullock, T. H., & Sejnowski, T. J. (2000b). Gap junction effects on precision and frequency of a model pacemaker network. *Journal of Neurophysiology*, 83, 984–997.
- Moortgat, K. T., Keller, C. H., Bullock, T. H., & Sejnowski, T. J. (1998). Submicrosecond pacemaker precision is behaviorally modulated: the gymnotiform electromotor pathway. *Proceedings* of the National Academy of Sciences U.S.A., 95, 4684–4689.
- Selverston, A. I. (2010). Invertebrate central pattern generator circuits. *Philosophical Transactions of the Royal Society B*, 365, 2329–2345.
- Sîrbulescu, R. F., Ilieş, I., & Zupanc, G. K. H. (2014). Quantitative analysis reveals dominance of gliogenesis over neurogenesis in an adult brainstem oscillator. *Developmental Neurobiology*, 74, 934–952
- Stiefel, K. M., & Ermentrout, G. B. (2016). Neurons as oscillators. *Journal of Neurophysiology*, 116, 2950–2960.
- Tattini, L., Olmi, S., & Torcini, A. (2012). Coherent periodic activity in excitatory Erdös-Renyi neural networks: The role of network connectivity. *Chaos*, 22, 023133.
- Tönjes, R., Masuda, N., & Kori, H. (2010). Synchronization transition of identical phase oscillators in a directed small-world network. *Chaos*, 20, 033108.
- Vasalou, C., Herzog, E. D., & Henson, M. A. (2009). Small-world network models of intercellular coupling predict enhanced synchronization in the suprachiasmatic nucleus. *Journal of Biological Rhythms*, 24, 243–254.
- Waxman, S. G., Pappas, G. D., & Bennett, M. V. L. (1972). Morphological correlates of functional differentiation of nodes of Ranvier along single fibers in the neurogenic electric organ of the knife fish Sternarchus. Journal of Cell Biology, 53, 210–224.
- White, J. A., Chow, C. C., Ritt, J., Soto-Treviño, C., & Kopell, N. (1998). Synchronization and oscillatory dynamics in heterogeneous, mutually inhibited neurons. *Journal of Computational Neuroscience*, 5, 5–16.
- Yamamoto, T., Maler, L., Hertzberg, E. L., & Nagy, J. I. (1989). Gap junction protein in weakly electric fish (Gymnotide [sic]): Immuno-histochemical localization with emphasis on structures of the electrosensory system. *Journal of Comparative Neurology*, 289, 509–536.
- Zupanc, G. K. H. (2018). Electrocommunication. In J. P. Stein (Ed.), Reference module in neuroscience and biobehavioral psychology (pp. 1–13). Elsevier.
- Zupanc, G. K. H., Amaro, S. M., Lehotzky, D., Zupanc, F. B., & Leung, N. Y. (2019). Glia-mediated modulation of extracellular potassium concentration determines the sexually dimorphic output frequency of a model brainstem oscillator. *Journal of Theoretical Biology*, 471, 117–124.
- Zupanc, G. K. H., & Bullock, T. H. (2005). From electrogenesis to electroreception: An overview. In T. H. Bullock, C. D. Hopkins,
 A. N. Popper, & R. R. Fay (Eds.), *Electroreception* (pp. 5–46).
 Springer Science + Business Media.
- Zupanc, G. K. H., Ilieş, I., Sîrbulescu, R. F., & Zupanc, M. M. (2014). Large-scale identification of proteins involved in the development of a sexually dimorphic behavior. *Journal of Neurophysiology*, 111, 1646–1654.
- Zupanc, G. K. H., & Maler, L. (1993). Evoked chirping in the weakly electric fish Apteronotus leptorhynchus: A quantitative biophysical analysis. Canadian Journal of Zoology, 71, 2301–2310.



Zupanc, G. K. H., Sîrbulescu, R. F., Nichols, A., & Ilies, I. (2006). Electric interactions through chirping behavior in the weakly electric fish, *Apteronotus leptorhynchus*. *Journal of Comparative Physiology A*, 192, 159–173.

Publisher's Note Springer Nature remains neutral with regard to jurisdictional claims in published maps and institutional affiliations.

Springer Nature or its licensor holds exclusive rights to this article under a publishing agreement with the author(s) or other rightsholder(s); author self-archiving of the accepted manuscript version of this article is solely governed by the terms of such publishing agreement and applicable law.

